Gain and Power Parameter Measurements Using Planar Near-Field Techniques

ALLEN C. NEWELL, SENIOR MEMBER, IEEE, ROBERT D. WARD, AND EDWARD J. MCFARLANE

Abstract—**Equations are derived and measurement techniques described for obtaining gain, effective radiated power, and saturating flux density using planar near-field measurements. These are compared with conventional far-field techniques, and a number of parallels are evident. These give insight to the theory and help to identify the critical measurement parameters. Application of the techniques to the INTELSAT VI satellite are described.**

Introduction

IT IS generally well known that the relative far-field pattern of an antenna is readily available from near-field measurements using either a planar, cylindrical, or spherical scan surface. It does not seem to be nearly as clear, however, that gain and other power-related parameters are included in the basic theory and that relatively few additional measurements are required to obtain them. There is also a persistent misunderstanding that since the near-to-far transformation involves an integration, directivity rather than gain is obtained, and is in error due to lack of information about far-out and back lobes. In the following, we will present the theory, measurements, and results for planar near-field measurements to help clarify these points and describe how gain and other power-related parameters are obtained. When correctly formulated, it is instructive to see how closely the working equations resemble similar far-field relations. We will describe three methods for obtaining gain, along with techniques for determining the effective isotropic radiated power (EIRP) of an antenna-transmitter system, and saturating flux density for an antenna–receiver system.

Theoretical Summary

We begin a discussion of gain and power-parameter measurements by reviewing the basic equations used in the plane-wave scattering matrix theory of antennas [1]. The transmission equations for the situation where the probes are receiving are

$$b_0'(\mathbf{P}) = F' a_0 \int \mathbf{t}_{10}(\mathbf{K}) \cdot \mathbf{s}_{02}'(\mathbf{K}) e^{i\gamma d} e^{i\mathbf{K}\cdot\mathbf{P}}\, d\mathbf{K} \quad (1)$$

$$b_0''(\mathbf{P}) = F'' a_0 \int \mathbf{t}_{10}(\mathbf{K}) \cdot \mathbf{s}_{02}''(\mathbf{K}) e^{i\gamma d} e^{i\mathbf{K}\cdot\mathbf{P}}\, d\mathbf{K}. \quad (2)$$

Manuscript received October 1987; revised January 1988.

A. C. Newell is with the Electromagnetic Fields Division, National Bureau of Standards, Boulder, CO 80303.

R. D. Ward is with the Space & Communications Group, Hughes Aircraft Company, P.O. Box 92919, Building S1, MS D347, Los Angeles, CA 90009.

E. J. McFarlane is with the System Test Engineering Laboratory, Hughes Aircraft Company, El Segundo, CA 90245.

IEEE Log Number 8821114.

In these equations, $b_0'(\mathbf{P})$ and $b_0''(\mathbf{P})$ represent the complex outputs of two probes that have nominally orthogonal polarizations, where $\mathbf{P}$ is the x, y position vector on the plane $z = d$, and a_0 is the input to the antenna under test (AUT) as illustrated schematically in Fig. 1. F' and F'' are impedance mismatch factors between the respective probes and the "load" port connected to the probes,

$$F' = \frac{1}{1-\Gamma_l \Gamma_p'} \qquad F'' = \frac{1}{1-\Gamma_l \Gamma_p''}, \quad (3)$$

where Γ_l, Γ_p', Γ_p'' are, respectively, the reflection coefficients of the load, the first probe, and the second probe. The transmitting properties of the AUT are specified by the plane-wave transmitting coefficients (PWTC) $\mathbf{t}_{10}(\mathbf{K})$, which are a function of the transverse part of the propagation vector $\mathbf{k}$,

$$\mathbf{K} = k_x \hat{x} + k_y \hat{y}, \quad (4)$$

and the magnitude of the z component of $\mathbf{k}$ is denoted by γ. In a similar way, $\mathbf{s}_{02}'(\mathbf{K})$ and $\mathbf{s}_{02}''(\mathbf{K})$ represent the plane-wave receiving coefficients (PWRC) of the two probes. Consistent with the notation employed by Kerns in the original development, the lower case s's and t's represent the *complete* vectors, not merely the x, y components.

The solution for the AUT parameters is accomplished by a combination of a Fourier transform of the measured data, and then a probe correction of the resulting angular spectra $D'(\mathbf{K})$ and $D''(\mathbf{K})$,

$$D'(\mathbf{K}) = \frac{e^{-i\gamma d}}{4\pi^2 F' A'} \int B_0'(\mathbf{P}) e^{-i\mathbf{K}\cdot\mathbf{P}}\, d\mathbf{P} \quad (5)$$

$$D''(\mathbf{K}) = \frac{e^{-i\gamma d}}{4\pi^2 F'' A''} \int B_0''(\mathbf{P}) e^{-i\mathbf{K}\cdot\mathbf{P}}\, d\mathbf{P} \quad (6)$$

$$t_{10m}(\mathbf{K}) = \frac{\dfrac{D'(\mathbf{K})}{s_{02m}'(\mathbf{K})} - \dfrac{D''(\mathbf{K})}{s_{02c}''(\mathbf{K})} \rho_s'(\mathbf{K})}{1-\rho_s'(\mathbf{K})/\rho_s''(\mathbf{K})} \quad (7)$$

$$t_{10c}(\mathbf{K}) = \frac{\dfrac{D''(\mathbf{K})}{s_{02c}''(\mathbf{K})} - \dfrac{D'(\mathbf{K})}{s_{02m}'(\mathbf{K})\rho_s''(\mathbf{K})}}{1-\rho_s'(\mathbf{K})/\rho_s''(\mathbf{K})}. \quad (8)$$

In these equations, some conventions have been employed for compactness. The first is to express the ratio $b_0'(\mathbf{P})/a_0$ as the

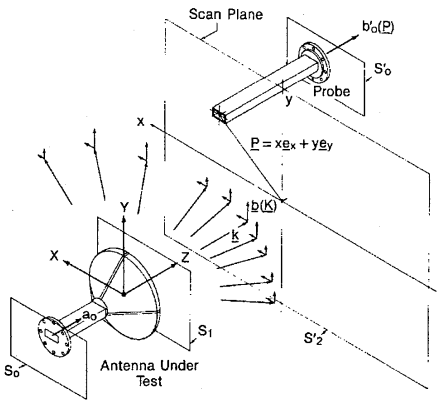

Fig. 1. Schematic of planar near-field measurement system.

ratio of relative near-field data,

$$B_0'(\mathbf{P}) = \frac{b_0'(\mathbf{P})}{b_0'(\mathbf{P}_0)}, \tag{9}$$

and the normalization constant

$$A' = \frac{a_0}{b_0'(\mathbf{P}_0)}. \tag{10}$$

The near-field amplitude and phase pattern can then be measured relative to the reference point $\mathbf{P}_0$, which is generally at or near the maximum amplitude, and the normalization constant can be measured in a separate procedure. More will be said about the normalization constant later because it is a very important part of gain and power parameter measurements. The second convention is the use of m and c subscripts on the plane-wave coefficients in (7) and (8). They are used to denote two orthogonal vector components of the vectors $\mathbf{t}_{10}(\mathbf{K})$ or $\mathbf{s}_{02}(\mathbf{K})$. They generally denote "main" and "cross" components; however, to be consistent with other definitions of polarization ratios, the m subscript specifically denotes either the linear components referred to as elevation, ϵ, vertical, ϕ, or the right-circular component. The c subscript then denotes the corresponding orthogonal components, azimuth, α, horizontal, θ, or left-circular [2]. As a general rule, the probes are chosen such that the first probe, $\mathbf{s}_{02}'(\mathbf{K})$, couples primarily to the m component, and the second one, $\mathbf{s}_{02}''(\mathbf{K})$, couples primarily to the c component.

The plane-wave scattering matrix coefficients are power normalized [1] so that *absolute* quantities such as power gain, receiving area, ohmic loss, and effective isotropic radiated power (EIRP) follow directly from a solution for $\mathbf{t}_{10}(K)$. The defining equations for the basic quantities are

$$G(\mathbf{K}) = \frac{4\pi Y_0 \gamma^2 |\mathbf{t}_{10}(\mathbf{K})|^2}{\eta_0(1-|\Gamma_a|^2)} \tag{11}$$

$$\sigma(\mathbf{K}) = \frac{4\pi^2 \eta_0 |\mathbf{s}_{02}'(\mathbf{K})|^2}{Y_0(1-|\Gamma_p'|^2)} \tag{12}$$

where $G(\mathbf{K})$ denotes the power-gain function, $\sigma(\mathbf{K})$ is the receiving effective area, $Y_0 = \sqrt{\epsilon/\mu}$ is the plane-wave admittance in the space medium, η_0 is the characteristic admittance for propagated waves in the transmission line connected to the antennas, and Γ_a is the AUT's reflection coefficient.

Gain Measurements

Three basic methods exist for obtaining absolute power gain from planar near-field measurements. They are referred to as 1) the direct gain measurement, 2) the gain comparison technique, and 3) the three-antenna measurement. In all three methods, three quantities enter into the calculation of the AUT's gain. These are one or more sets of relative near-field data such as $B_0'(\mathbf{P})$, the gain of a standard antenna, and one or more power ratio or insertion loss measurements such as A' or A'' in (5) and (6). The three techniques differ in how the gain standard is employed, and in the number and type of near-field and power-ratio measurements.

Direct Gain Measurement

The first method is called a direct gain measurement because it is based on a direct application of the basic equations and the probe is used as the gain standard. In (11) and (12), both $\mathbf{t}_{10}(\mathbf{K})$ and $\mathbf{s}_{02}'(\mathbf{K})$ are absolute parameters, with dimensions of length, and are not simply quantities normalized to some maximum value. Therefore, if $\mathbf{t}_{10}(\mathbf{K})$ is obtained, the gain follows directly from (11). Since $\mathbf{t}_{10}(\mathbf{K})$ is found from the probe correction (7) and (8), it follows that $\mathbf{s}_{02}'(\mathbf{K})$, $\mathbf{s}_{02}''(\mathbf{K})$, $D'(\mathbf{K})$, and $D''(\mathbf{K})$ must also be absolute rather than relative parameters. We will now describe the steps involved in determining each of these quantities. The details of obtaining the PWRC for both probes are discussed elsewhere [2]. It is sufficient to note here that the correct magnitude and dimension of $\mathbf{s}_{02}'(\mathbf{K})$ are achieved through knowing the probe gain and using (12). From measurements of the probe's gain $G_p'(0)$, polarization ratio $\rho_s'(0)$, and reflection coefficient Γ_p', and using the relation $\sigma_p(0) = \lambda^2 G_p(0)/4\pi$, which holds for reciprocal antennas,

$$|s_{02m}'(0)| = \left| \frac{y_0(1-|\Gamma_p'|^2)G_p'(0)}{\eta_0 4\pi k^2 (1+|\rho_s'(0)|^2)} \right|^{1/2}. \tag{13}$$

Here, we assume that the m component is the main component for the first probe. From similar information about the second probe, we obtain $|s_{02c}''(0)|$, again assuming that the c component is the main component for the second probe. In the special, but frequent case when the "second" probe is obtained by a 90° rotation of a linearly polarized probe, $s_{02m}'(0) \equiv s_{02c}''(0)$.

The measured near-field data are referenced to the input amplitude and phase as outlined in (1), (2), (5), and (6) by the normalization constants A' and A'' as defined by (10). These constants are obtained from amplitude and phase insertion loss measurements. The usual approach to obtain A' is to place the probe at $\mathbf{P}_0$, set the receiver outputs to 0 dB (or some convenient level), connect the "generator" and "load" ports directly together as illustrated in Fig. 2, and observe the change in amplitude and phase. We denote the resulting

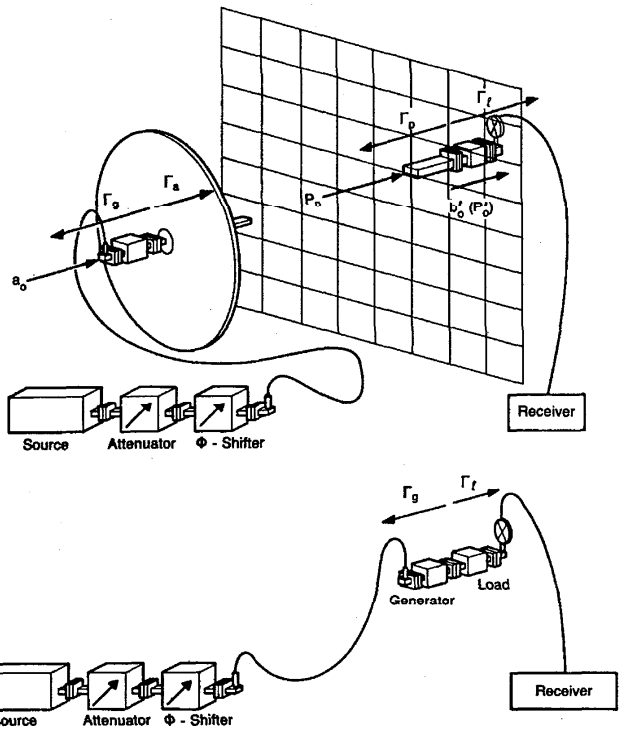

Fig. 2. Schematic of insertion loss measurement showing generator and load ports connected to antennas and to each other.

amplitude and phase changes by a_n' and ψ_n', respectively; then

$$A' = \frac{a_0}{b_0'(\mathbf{P}_0)} = \frac{(1-\Gamma_g\Gamma_l)}{(1-\Gamma_g\Gamma_a)}\, a_n' e^{i\psi_n'}, \tag{14}$$

where Γ_g and Γ_l are the reflection coefficients for the generator and load ports. The amplitude change is most accurately measured with a calibrated attenuator as shown in Fig. 2 to reproduce the original level when generator and load are connected together.

The magnitude of this insertion loss is approximately equal to the ratio of the AUT maximum gain to probe gain,

$$(a_n')^2 \approx \frac{G_a(\mathbf{K}_0)}{G_p(\mathbf{K}_0)},$$

and for typical antennas and probes is on the order of 25–40 dB. Since any error in this insertion loss causes an identical error in the gain of the AUT, it is important to measure a_n' as accurately as possible. The source output a_0 must remain constant during the measurement, and the mixer must be well isolated and stable. To improve accuracy, the measurement is generally repeated a few times to make sure that connectors are repeatable and measurements consistent to a few hundredths of a decibel. Another approach to improving gain accuracy is to use as large a probe as possible without increasing multiple reflection errors and filtering desired parts of the wide angle pattern. The larger probe will increase signal-to-noise ratio, reduce the magnitude of a_n' and therefore improve its accuracy, and also reduce probe-gain error.

The parameter A'' can be obtained from a similar process with the second probe at $\mathbf{P}_1$. If a single probe is used with either rotation or polarization switching, A'' is also conveniently measured from the ratio of the probe outputs due to the combined changes in "probes" and position from $\mathbf{P}_0$ to $\mathbf{P}_1$:

$$A'' = A' \frac{b_0'(\mathbf{P}_0)}{b_0''(\mathbf{P}_1)}. \tag{15}$$

This approach eliminates the movement of the generator and load ports a second time, and the observed amplitude change will generally be less, thereby improving its accuracy. That is,

$$\left|\frac{b_0'(\mathbf{P}_0)}{b_0''(\mathbf{P}_1)}\right| < |a_n''|. \tag{16}$$

The quantities b_0' and b_0'' are the outputs at the probe terminals. The insertion losses must be measured at these terminals and calibration of the probes must include adapters, connectors, etc., up to these terminals. If a dual-mode probe and switching are used, the transmission line to the switch must either be considered a part of the probe or properly accounted for in determining A' and A''.

The insertion loss measurement usually requires either moving and flexing the transmission line, inserting a substitute section of line with known properties, or removing the AUT

and probe and translating of the support tower for direct connection. The antenna type and frequency will generally dictate the best method. At frequencies where flexible line or rotary joints can be used without introducing significant signal changes, this is an attractive choice, for then the alignment and mounting of the AUT are not disturbed and the measurement can be repeated quickly to improve accuracy. If the insertion loss technique is not feasible, power measurements at the generator and load ports with the appropriate impedance mismatch correction will give the magnitude of A' and its phase is arbitrary. A'' can then be found from the ratio technique, (15).

To understand the factors affecting gain measurements, we note the form of the gain equation for a special, and yet very frequently encountered, example of the direct measurement. The special case assumes that the probe is polarization matched to the AUT in the direction of the AUT main beam. Specifically, if the main beam is in the direction $\mathbf{K}_0$ and the probe is polarization matched to the AUT for $\mathbf{K}_0$, (5), (7), (11), (13), and (14) reduce to

$$G_a(\mathbf{K}_0) = \left(\frac{4\pi}{\lambda^2}\right)^2 \frac{|1-\Gamma_l\Gamma_p|^2}{(1-|\Gamma_a|^2)(1-|\Gamma_p|^2)} \frac{|b_0'(\mathbf{P}_0)|^2}{|a_0|} \cdot \frac{|\delta_x\delta_y\Sigma_i B_0'(\mathbf{P}_i)e^{-i\mathbf{K}_0\cdot\mathbf{P}_i}|^2}{G_p(\mathbf{K}_0)} \tag{17a}$$

$$= \left(\frac{4\pi}{\lambda^2}\right)^2 \frac{|1-\Gamma_l\Gamma_p|^2|1-\Gamma_g\Gamma_a|^2}{|1-\Gamma_g\Gamma_l|^2(1-|\Gamma_a|^2)(1-|\Gamma_p|^2)} \cdot \frac{|\delta_x\delta_y\Sigma_i B_0'(\mathbf{P}_i)e^{-i\mathbf{K}_0\cdot\mathbf{P}_i}|^2}{|a_n'|^2 G_p(\mathbf{K}_0)} \tag{17b}$$

for the partial gain of the main component. Five factors determine the gain: 1) a constant involving the wavelength; 2) an impedance mismatch factor involving the various reflection coefficients which is typically on the order of 0.01–0.5 dB; 3) the complex sum of the relative near-field data, which can be thought of as approximately the "volume" under the near-field amplitude pattern for a collimated beam; 4) the insertion loss $|a_n'|^2$, and 5) the gain of the probe. Of these, the last three are by far the most important since their accuracy will ultimately determine the accuracy of the gain measurement.

For later applications, we compare the gain equation for near-field measurements to one for a hypothetical far-field measurement involving the same two antennas and the same assumption of polarization match. Assume that the probe is placed at a distance d_f in the far field of the AUT in a reflection-free environment. Further, assume that the input to the AUT is a_f and that by some means the far-field insertion loss

$$|A_f'|^2 = \left|\frac{a_f}{b_f(\mathbf{K}_0)}\right|^2 \tag{18}$$

is measured. The AUT gain is then obtained from the Friss transmission equation written in the following form to show its similarity to (17):

$$G_a(\mathbf{K}_0) = \left(\frac{4\pi}{\lambda^2}\right)^2 M_f \left|\frac{b_f(\mathbf{K}_0)}{a_f}\right|^2 \frac{(\lambda d_f)^2}{G_p(\mathbf{K}_0)}. \tag{19}$$

The impedance mismatch factor M_f will depend on how the insertion loss is measured. If it is measured in the same way as the near field, that is by connecting generator and load together, M_f will be identical to the mismatch factor in (17a). The equation for this measurement has four of the five factors noted for the near-field measurement, the probe gain and insertion loss have identical roles, and the product λd_f replaces the product of $\delta_x\delta_y$ times the sum of the near-field data. This comparison makes the near-field gain measurement less obscure and also provides two additional results that are useful in other applications. The first will be used in deriving the relation for near-field saturating flux density measurement and is obtained by equating (17a) and (19), since both represent the gain of the AUT. Canceling common factors gives the first result,

$$\left|\frac{b_0'(\mathbf{P}_0)a_f}{b_f(\mathbf{K}_0)a_0}\right| = \left|\frac{\lambda d}{\delta_x\delta_y\Sigma_i B'(\mathbf{P}_i)e^{-i\mathbf{K}_0\cdot\mathbf{P}_i}}\right|. \tag{20}$$

The second equation gives a new version or derivation of the near-zone correction for two arbitrary antennas. If we let the "far-field" distance d_f be the same as the near-field distance, the apparent gain calculated by the Friss transmission in (19) is no longer the actual gain. If we add a factor $N(d)$ to (19) to represent the near-zone correction, the modified relation now gives the true gain. Since $d_f = d$, the subscript can now be dropped, and since

$$a_f = a_0 \qquad b_f(\mathbf{K}_0) = b'(\mathbf{P}_0),$$

if we chose $\mathbf{P}_0$ to be along the direction $\mathbf{K}_0$. Equating the modified (19) and (17a) and solving for $N(d)$ gives

$$N(d) = \left|\frac{\int B_0(\mathbf{P}d)e^{-i\mathbf{K}_0\cdot\mathbf{P}}\,d\mathbf{P}}{\lambda d}\right|^2 \tag{21a}$$

$$= \left|\frac{\int b_0'(\mathbf{P}, d)e^{-i\mathbf{K}_0\cdot\mathbf{P}}}{\lambda d b_0'(\mathbf{P}_0, d)}\right|^2. \tag{21b}$$

Sample Results and Comparison with Other Measurement Techniques

The direct measurement technique has been used extensively on a wide variety of antennas with very good success. It has been used on reflectors, phased arrays, shaped-beam offset reflectors, and horn antennas. To verify consistency with other measurement techniques, a number of comparison tests have been conducted using the near-field technique and far-field methods on the same antenna. Examples of three such comparisons are shown in Table I.

Gain Comparison

The second method, a gain comparison technique, is useful in cases where neither the insertion loss nor the power

TABLE I
GAIN COMPARISON TESTS

Test Antenna	Frequency (GHz)	Measured Gain Using Far Field	Measured Gain Using Near Field
Scalar horn	8.0	22.03	22.05
Cassegrain reflector	60.0	46.30	46.42
Microstrip array	1.28	30.50	30.30

measurements to determine A' and A'' are practical, or when the probe gain is not known. In the special case where the probe and AUT are polarization matched, the development of the gain equation is simplified by using (17). An abbreviated form of this equation for the probe AUT combinations is

$$G_a(\mathbf{K}_0) = CM_{ap} \frac{|\delta_x \delta_y \Sigma_{i\,ap} B_0'(\mathbf{P}_i) e^{-i\mathbf{K}_0 \cdot \mathbf{P}_i}|^2}{|A'_{ap}(\mathbf{P}_0)|^2 G_p(\mathbf{K}_0)}. \quad (22)$$

A similar relation for the same probe measuring a standard antenna whose gain in the direction $\mathbf{K}_0$ is known is

$$G_s(\mathbf{K}_0) = CM_{sp} \frac{|\delta_x' \delta_y' \Sigma_{i\,sp} B_0'(\mathbf{P}_i) e^{-i\mathbf{K}_0 \cdot \mathbf{P}_i}|^2}{|A'_{sp}(\mathbf{P}_2)|^2 G_p(\mathbf{K}_0)}. \quad (23)$$

Here, C is the constant $(4\pi/\lambda^2)^2$, M is the mismatch factor, the ap and sp subscripts denote, respectively, the quantities for the AUT-probe and standard-probe measurement. We have made the normalization points $\mathbf{P}_0$ and $\mathbf{P}_2$ explicit in the reference to the normalization constants to show that they do not have to be the same point for the two antennas. The z-separation distance in the two measurements may also be different since it does not appear in the gain equations. Taking the ratio of (22) and (23) and solving for $G_a(\mathbf{K}_0)$ gives

$$G_a(\mathbf{K}_0) = \frac{(1-|\Gamma_s|^2)|\delta_x \delta_y \Sigma_{i\,ap} B_0'(\mathbf{P}_i) e^{-i\mathbf{K}_0 \cdot \mathbf{P}_i}|^2}{(1-|\Gamma_a|^2)|\delta_x' \delta_y' \Sigma_{i\,sp} B_0'(\mathbf{P}_i) e^{-i\mathbf{K}_0 \cdot \mathbf{P}_i}|^2} \cdot \frac{|_s a_{0\,ap} b_0'(\mathbf{P}_0)|^2}{|_a a_{0\,sp} b_0'(\mathbf{P}_2)|^2} G_s(\mathbf{K}_0). \quad (24)$$

We note for comparison the gain equation for a far-field gain comparison measurement,

$$G_a(\mathbf{K}_0) = \frac{(1-|\Gamma_s|^2)(\lambda d_{ap})^2}{(1-|\Gamma_a|^2)(\lambda d_{sp})^2} \frac{|_s a_{0\,ap} b_f(\mathbf{K}_0)|^2}{|_a a_{0\,sp} b_f(0)|} G_s(0). \quad (25)$$

Here, d is the separation distance, a_0 the input, and b_f the output signals. The ap, a, and sp, s subscripts denote, respectively, the AUT-probe and standard-probe combinations. The similarity to (24) is again striking with λd replacing the near-field data sum, lattice area product.

In the more general case where both sets of near-field data are required for accurate gain calculation, such as when a linear probe is used to measure a circularly polarized test antenna, a more general treatment is required. The details for this situation can be found in [3]. In summary, gain comparison requires relative near-field measurements of the AUT and standard using the same probe, the gain of the standard, and the relative amplitude measurement implied by (24). To be successful, a series of steps must be carried out in a relatively short time. The inputs between the AUT and the standard must be switched, the two antennas accurately positioned and aligned, and the probe moved between $\mathbf{P}_0$ and $\mathbf{P}_2$. Simultaneously mounting both the AUT and standard on the positioning tower, either in opposite z directions or side by side, facilitates these changes.

Although this approach has certain advantages, it can increase some error sources. For example, if the standard is much smaller than the AUT, multiple reflection and truncation errors in ${}_{sp}B_0'(\mathbf{P})$ can be significant. This is illustrated in the results of a comparison measurement where the AUT was a 1.2-m reflector, the standard a pyramidal horn, and the probe an open-ended waveguide. The AUT and the horn were mounted on opposite ends of a rotator to allow for rapid positioning and alignment. The measurement was repeated at a sequence of z distances to evaluate the effect of multiple reflections with the results shown in Fig. 3. As shown, a direct gain measurement was also carried out to check on consistency and accuracy. Table II shows an estimate of errors for the two types of measurements.

Three-Antenna Measurement

The third method is a three-antenna measurement where two different probes are used and near-field scans are made for all three antenna combinations. If insertion loss measurements are made with each combination, the three gain equations are

$$G_a(\mathbf{K}) G_{p1}(0) = {}_f G_{ap1}(\mathbf{K}) \quad (26a)$$

$$G_a(\mathbf{K}) G_{p2}(0) = {}_f G_{ap2}(\mathbf{K}) \quad (26b)$$

$$G_{p1}(0) G_{p2}(0) = {}_f G_{p1p2}(0). \quad (26c)$$

The gains on the right of (26) are obtained by using the fictitious value of 1 for the probe gain in the data processing, or in the case of polarization match, solving for the gain product of the AUT and probe in (17). The subscripts ap1, ap2, and p1p2 denote, respectively, the three configurations, AUT-probe 1, AUT-probe 2, and probe 1–probe 2. From these three equations, $G_a(\mathbf{K})$, $G_{p1}(0)$, and $G_{p2}(0)$ are found. However, if the insertion loss is measured for the first pair and a relative amplitude measured between the second and third pairs as in the comparison measurement, the resulting equations are

$$G_a(\mathbf{K}) G_{p1}(0) = {}_f G_{ap1}(\mathbf{K}) \quad (27)$$

$$\frac{G_a(\mathbf{K})}{G_{p1}(0)} = \frac{{}_f G_{ap2}(K)}{{}_f G_{p1p2}(0)} \left| \frac{A'_{p1p2}}{A'_{ap2}} \right| \quad (28)$$

and only $G_a(\mathbf{K})$ and $G_{p1}(0)$ are obtainable. This technique is seldom used because it requires three near-field scans, and the probe-to-probe measurement produces relatively large errors due to multiple reflections and truncation.

SYSTEM POWER PARAMETERS

In addition to antenna gain, two other system power parameters associated with communication satellites are also easily obtained from the near-field measurements. These are the effective isotropic radiated power (EIRP) and saturating

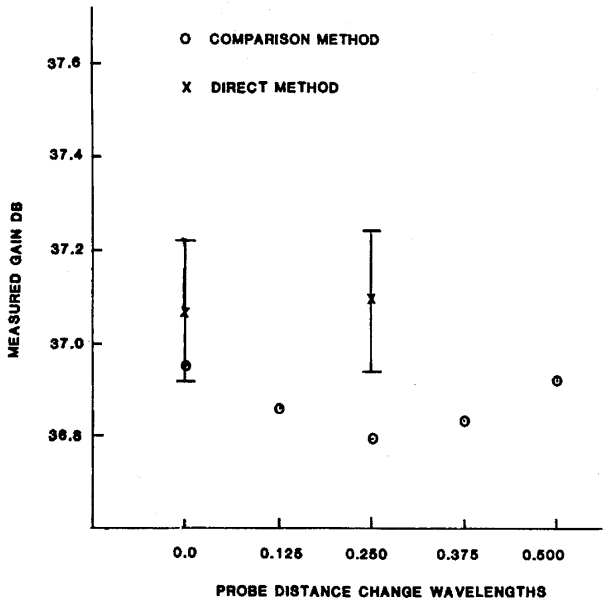

Fig. 3. Results of comparison gain measurements taken at series of z distances.

TABLE II
ERROR ESTIMATES FOR DIRECT AND COMPARISON GAIN MEASUREMENTS

Source of Error	Estimated error Direct	Comparison
Probe or standard gain uncertainty	0.10	0.10
Insertion loss or comparison amplitude error	0.08	0.05
Amplitude nonlinearity	0.05	0.05
Multiple reflections	0.05	0.10
Position errors	0.01	0.01
Measurement area truncation	0.05	0.15
Phase error	0.01	0.01
RSS Combination	0.16	0.22

flux density. These measurement will be described for the case when the probe is polarization matched to the AUT and therefore $D''(\mathbf{K})$ does not make a significant contribution to the determination of $t_{10m}(\mathbf{K})$ and $G_a(\mathbf{K})$.

EIRP is defined as the product of the antenna gain and the net input power to the antenna. It may then be determined from two measurements; the gain from near-field techniques and the input power using a power meter. Both of these require access to the input port of the AUT and measurements at this terminal. In satellite applications, it is often desirable to measure the total system performance without breaking the connection between the AUT and the transmitter. This is accomplished on a far-field range from a knowledge of the gain of the standard antenna G_s, the range separation distance d, and the power received by the standard antenna $\mathcal{P}_R$. The EIRP is

$$\text{EIRP} = (4\pi)^2 \frac{\mathcal{P}_R}{G_s} \left(\frac{d}{\lambda}\right)^2 . \tag{29}$$

To obtain the near-field relations for measurement without access to the AUT input port, we note that the net input power to the AUT is

$$\mathcal{P}_i = \frac{\eta_0 |a_0|^2 (1 - |\Gamma_a|^2)}{2} \tag{30}$$

and the net output power from the probe, when it is at the reference position, is

$$\mathcal{P}_0(\mathbf{P}_0) = \frac{\eta_0 |b_0'(\mathbf{P}_0)|^2 (1 - |\Gamma_l|^2)}{2} . \tag{31}$$

The EIRP in the direction denoted by $\mathbf{K}_0$ is then obtained from the product of $G_a(\mathbf{K})$ and $\mathcal{P}_i$ in a way similar to the derivation of (17);

$$\text{EIRP}(\mathbf{K}_0) = (4\pi)^2 \left(\frac{|1 - \Gamma_l \Gamma_\rho|^2 \mathcal{P}_0(\mathbf{P}_0)}{(1 - |\Gamma_p|^2)(1 - |\Gamma_l|^2) G_p(\mathbf{K}_0)} \right) \cdot \left(\frac{|\delta_x \delta_y \Sigma_i B_0'(\mathbf{P}_i) e^{-i\mathbf{K}_0 \cdot \mathbf{P}_i}|^2}{\lambda^4} \right) . \tag{32}$$

The EIRP is then obtained from the relative near-field data $B_0'(\mathbf{P})$ used to obtain the patterns and a measurement of the probe output power at the reference point.

The flux density required to saturate the system receiver is normally measured on a far-field range and is given in terms of the net input power $\mathcal{P}_i$, and the gain G_s of the source antenna by the relation

$$S_0 = \frac{\mathcal{P}_i G_s}{4\pi d^2} . \tag{33}$$

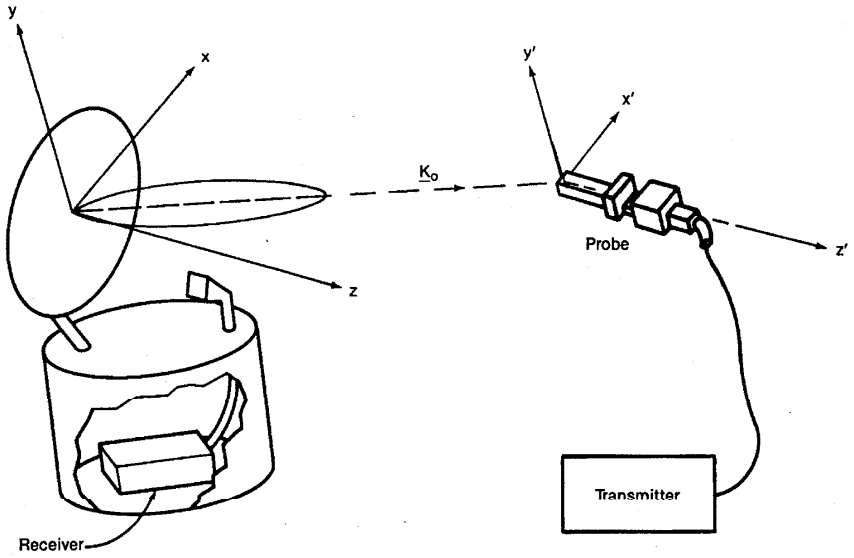

Fig. 4. Hypothetical far-field measurement using probe as source.

The power input to the source is that sufficient to saturate the receiver.

The development of a similar near-field equation begins with the concept of placing the probe on a far-field range in place of the source antenna, as shown in Fig. 4. In the general case, the main beam of the AUT is at $\mathbf{K}_0$ and may not be along the antenna's z axis; the probe is also rotated by the same amount so the gain of the probe appearing in (33) is $G_p(\mathbf{K}_0)$. Using (30) and (33), the flux density for this hypothetical situation is

$$S_0=\frac{\mathcal{P}_i G_p(\mathbf{K}_0)}{4\pi d^2}=\frac{\eta_0|a_f|^2(1-|\Gamma_p|^2)G_p(\mathbf{K}_0)}{8\pi d^2}. \tag{34}$$

In principle, the gain of the antenna could be obtained from this far-field measurement using the Friss transmission equation,

$$G_a(\mathbf{K}_0)=\left(\frac{4\pi}{\lambda^2}\right)^2 M_f\left|\frac{b_f(\mathbf{K}_0)}{a_f}\right|^2\frac{(\lambda d)^2}{G_p(\mathbf{K}_0)}. \tag{35}$$

Here, a_f is the input to the probe that produces the output at the AUT $b_f(\mathbf{K}_0)$ which is sufficient to saturate the receiver. The f subscripts denote the far field measurement situation and $\mathbf{K}_0$ denotes the direction of the main beam for the AUT.

If the AUT and the probe are now placed on a near-field range in the usual orientation and data obtained for the near-field gain equation, the antenna gain from (17a) is

$$G_a(\mathbf{K}_0)=\left(\frac{4\pi}{\lambda^2}\right)^2 M\left|\frac{b_n(\mathbf{P}_0)}{a_n}\right|^2\frac{|\delta_x\delta_y\Sigma_i B_0'(\mathbf{P}_i)e^{-i\mathbf{K}_0\cdot\mathbf{P}_i}|^2}{G_p(\mathbf{K}_0)}. \tag{36}$$

If the input to the probe a_n is adjusted so that the receiver is again saturated,

$$|b_n(\mathbf{P}_0)|^2=|b_f(\mathbf{K}_0)|^2 \tag{37}$$

and therefore

$$|a_f|^2=|a_n|^2\frac{(\lambda d)^2}{|\delta_x\delta_y\Sigma_i B_0'(\mathbf{P}_i)e^{-i\mathbf{K}_0\cdot\mathbf{P}_i}|^2}. \tag{38}$$

Substituting this value of $|a_f|^2$ into (34) gives the equation for near-field measurement of saturating flux density:

$$S_0=\left(\frac{\eta_0|a_n|^2(1-|\Gamma_p|^2)G_p(\mathbf{K}_0)}{8\pi}\right)\cdot\left(\frac{\lambda^2}{|\delta_x\delta_y\Sigma_i B_0'(\mathbf{P}_i)e^{-i\mathbf{K}_0\cdot\mathbf{P}_i}|^2}\right) \tag{39a}$$

$$=\left(\frac{\mathcal{P}_i G_p(\mathbf{K}_0)}{4\pi}\right)\left(\frac{\lambda^2}{|\delta_x\delta_y\Sigma_i B_0'(\mathbf{P}_i)e^{-i\mathbf{K}_0\cdot\mathbf{P}_i}|^2}\right). \tag{39b}$$

This equation has been obtained by considering hypothetical far-field and near-field gain measurements which require power ratio measurements such as $|b_n(\mathbf{P}_0)/a_n|^2$. The final equation for flux density does not require such power ratios, however, or access to the output port of the AUT. Only the usual near-field data and the probe input power measurement are required.

The first application of near-field techniques to the measurement of EIRP and saturating flux density was accomplished at Hughes Aircraft Company[1] in El Segundo, CA. The measurement facility was designed for the INTELSAT[2] VI satellite

[1] Reference to Hughes Aircraft does not imply endorsement by the National Bureau of Standards.

[2] The INTELSAT spacecraft is being developed by an international team of contractors for the International Telecommunications Satellite Organization (INTELSAT). The views expressed herein are not necessarily those of INTELSAT.

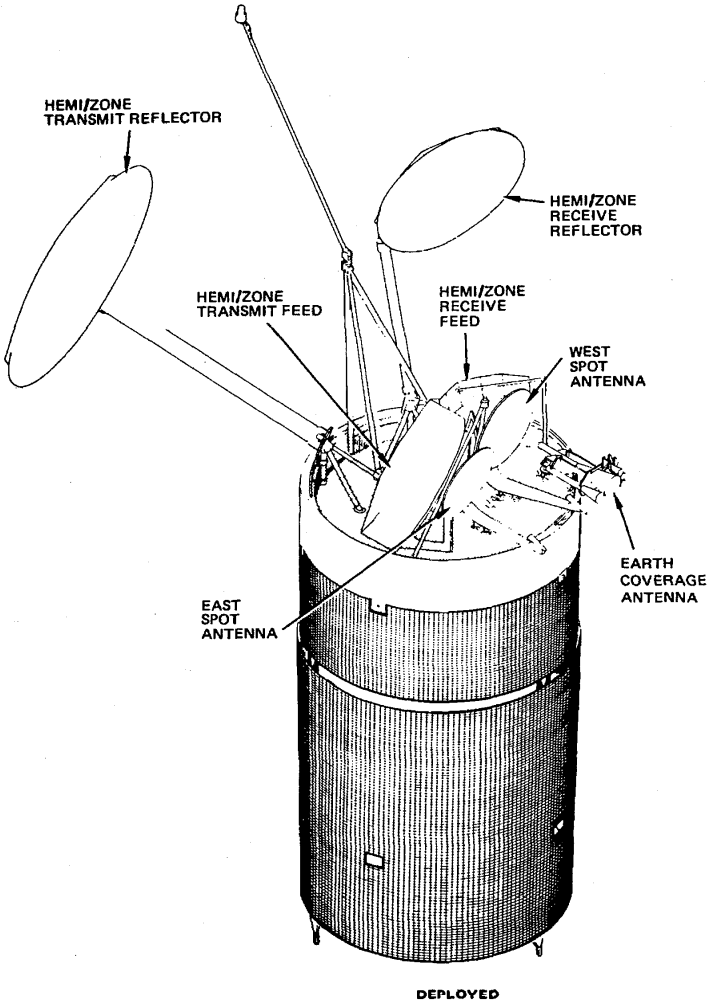

Fig. 5. INTELSAT VI satellite.

and has been used on a number of other satellites as well. Located at the Space and Communication Group headquarters, it provides an excellent environment for satellite testing. Environmental factors are carefully controlled, and the antennas are supported in a fixed position during the testing. Additionally, it is adjacent to the subsystem and system integration facilities, and the antenna tests can be accomplished without the transportation and handling required on a far-field range.

The planar measurement system covers an area of 6.4 m on each side, with scan speeds of 3.8 and 8.9 m/min, respectively, in the x and y directions. The probe position is measured with a laser interferometer with resolution of 1 μm. In its present configuration, the system will perform measurements in the frequency bands from 1.5 to 14.5 GHz.

The INTELSAT VI satellite shown in Fig. 5 is the world's largest and most complex commercial communication satellite. It is spin stabilized and designed to operate in one of three geosynchronous orbital regions. The RF payload is mounted on the despun section of the satellite, and consists of 50 communication transponders covering *C* band (6 GHz uplink/4 GHz downlink) and *Ku* band (14 GHz uplink/11 GH downlink). The RF system is visible below the antennas as the system is configured for near-field testing in Fig. 6. The antenna subsystem consists of two spotbeam antennas, two global communication antennas, and two large hemi/zone feed networks along with their offset reflectors. The hemi/zone feed arrays simultaneously form six beams. These include four zone beams shaped for the particular land areas covered, and two hemispheric beams. The networks are reconfigured for each of the three geosynchronous orbital locations to produce beams appropriate for the earth coverage region. This reconfi-

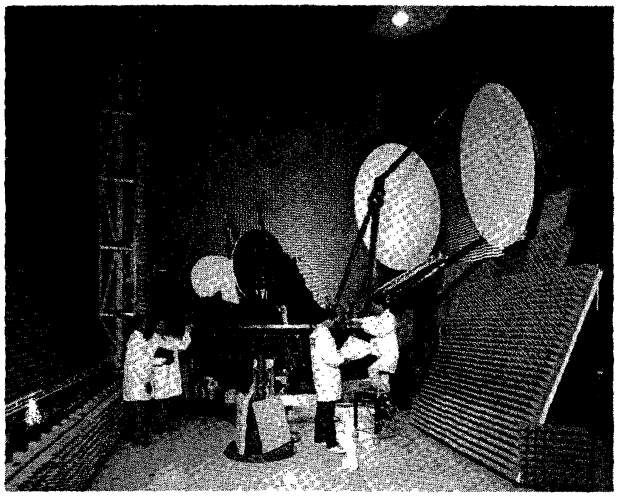

Fig. 6. INTELSAT VI satellite on planar near-field range showing RF and antenna systems.

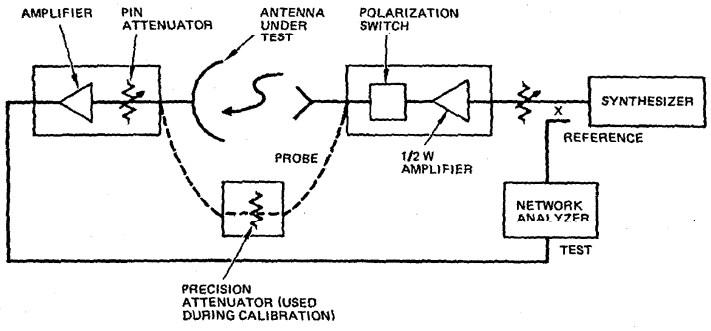

Fig. 7. Measurement system schematic for gain measurements.

guration is accomplished by means of a switching network in the transmission line that adjusts the amplitude and phase to each of the feed elements.

The direct gain measurement technique was used when only the antennas (without the RF system) were being tested, and access was available at the input or output of the feeds. Fig. 7 is a schematic of the test setup. The results of one measurement are shown in Table III, along with comparison to a similar far-field test.

Figs. 8 and 9 show the test setup for the EIRP and flux density measurements. Relative near-field data ($B_0'(\mathbf{P})$) were obtained in the usual manner using the location of the maximum amplitude as the reference point $\mathbf{P}_0$. The probe was then placed at this point for the power measurements. In saturating flux density measurements, the power input to the probe was gradually increased until the transponder under test

TABLE III
SAMPLE GAIN RESULTS FOR SPOT BEAM ANTENNA

Channel	Mode	Frequency (MHz)	Gain (dB)[a] From Near-Field Measurements	Gain (dB) From Far-Field Measurements
1, 2	Rx	10992.5	40.92	41.55
5, 6	Rx	11155.0	40.94	41.55
9–12	Rx	11618.5	41.22	41.40
1, 2	Tx	14042.5	42.12	42.74
5, 6	Tx	14205.0	42.02	42.55
7, 8	Tx	14418.5	42.02	42.70

[a] Uncalibrated piece of waveguide included in measurement. Estimate 0.3 dB loss.

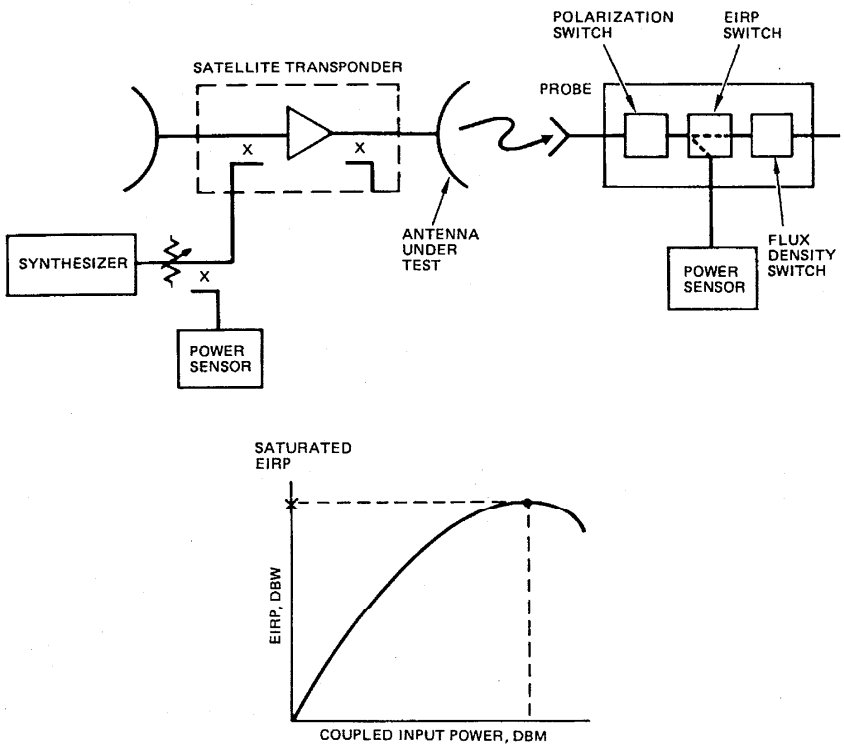

Fig. 8. Measurement system schematic for EIRP measurement.

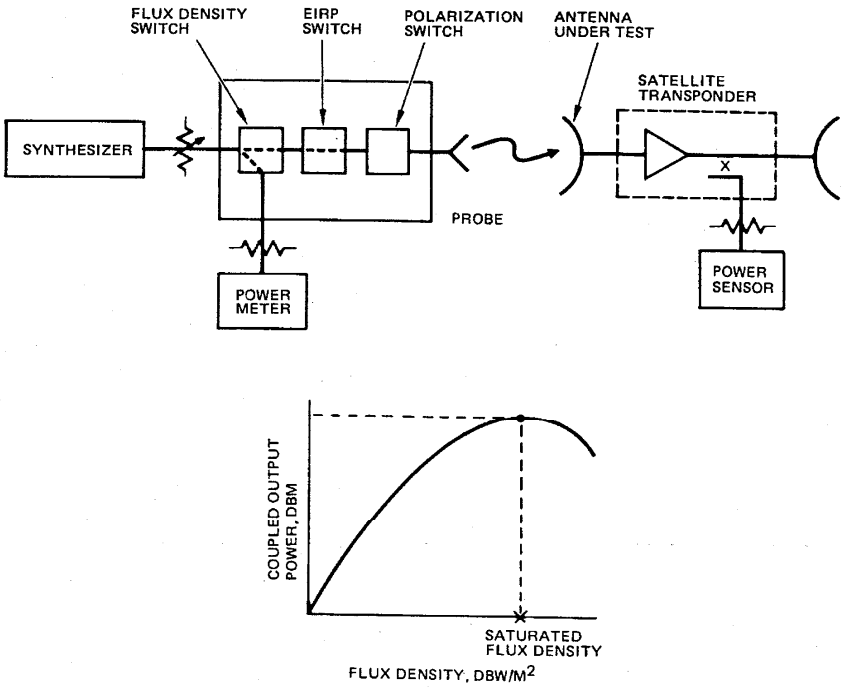

Fig. 9. Measurement system schematic for saturating flux density measurement.

TABLE IV
SATURATING FLUX DENSITY MEASUREMENT RESULTS FOR INTELSAT VI ANTENNAS

Antenna	Channel	Measured SFD (dBW/m²)	Predicted SFD (dBW/m²)	Delta
Global A	9	−81.49	−81.88	+0.39
Global A	10	−81.15	−81.41	+0.26
Global A	11	−81.29	−81.6	+0.31
Global A	12	−81.83	−81.76	−0.07
Zone 1	1-2	−81.39	−81.35	−0.04
Zone 1	3-4	−81.41	−81.10	−0.31
Zone 1	5-6	−81.30	−81.50	+0.20
Zone 1	7-8	−81.80	−82.00	+0.20
Zone 1	9	−81.92	−82.20	+0.28

TABLE V
SAMPLE RESULTS FOR INTELSAT VI EIRP MEASUREMENTS

Antenna	Channel	Measured EIRP (dB·W)	Predicted EIRP (dB·W)	Delta
East spot	1, 2	45.05	45.30	−0.25
West spot	5, 6	48.25	48.90	−0.65
East hemi	3, 4	35.37	35.40	−0.03
West hemi	7, 8	34.70	34.50	+0.20
Zone 1	3, 4	35.90	36.20	−0.30
Zone 4	1, 2	35.28	35.25	+0.03

TABLE VI
COMPARISON OF ESTIMATED AND MEASURED POWER LEVELS IN EIRP AND SATURATING FLUX DENSITY MEASUREMENTS

Freq (GHz)	AUT Gain (dB)	Probe Gain (dB)	Flux Density Power (dBmW) Estimated	Flux Density Power (dBmW) Measured	EIRP Power (mW) Estimated	EIRP Power (mW) Measured
3.905	34.4	12.8	—	—	10.5	6.0
6.13	32.5	12.2	−36.4	−29.7	—	—

in the satellite reached saturation. Saturation was detected by monitoring output power at the repeater test coupler. When saturation was observed, the power input to the probe was measured and used in (39b) along with the relative near-field data to calculate saturating flux density. A sample of results along with expected performance as predicted from design parameters and component tests are itemized in Table IV.

Measurement of the system EIRP is similar to the saturating flux density. After completing the relative near-field measurements, the probe was placed at the reference point. Power input to the transponder receive test coupler was gradually increased causing the transmit signal from the satellite to increase. When saturation of the repeater under test was indicated by the probe receive power remaining constant, the receive power was measured with the power meter. This value, along with the relative near-field data, was then used in (32) to obtain EIRP. Sample results are itemized in Table V. The estimates of uncertainty for both of these parameters are similar to those for gain, except that power measurement replaces the insertion loss or normalization constant. The uncertainty in the power measurements depends partly on the power level being measured. This can be estimated using (32) and (39b) and the approximation

$$|\delta_x \delta_y \Sigma_i B_0'(\mathbf{P}_i) e^{-i\mathbf{K}_0 \cdot \mathbf{P}_i}|^2 \approx A_e^2, \tag{40}$$

where A_e is the AUT's effective area.

The approximate power input to the probe for saturating flux density measurements is then

$$\mathcal{P}_i \approx \frac{\lambda^2 S_0 G_a^2}{4\pi G_p} \tag{41}$$

and the approximate power received by the probe in EIRP measurements is

$$\mathcal{P}_0 \approx \frac{(\text{EIRP})\ G_p}{G_a^2} \tag{42}$$

where G_p is the probe gain and G_a is the AUT gain. For the present measurements the gains, along with the estimated and actual power levels are noted in Table VI.

For these power levels, the estimated uncertainty in each of these measurements is itemized in Table VII.

TABLE VII
ESTIMATE OF ERRORS FOR SATURATING FLUX DENSITY AND EIRP MEASUREMENTS

Source of Error	Estimated Error (dB) for SFD Measurements	EIRP Measurements
Probe gain	0.10	0.10
Power measurement	0.20	0.20
Receiver nonlinearity	0.05	0.05
Multiple reflections	0.05	0.05
Position errors	0.01	0.01
Measurement area truncation	0.05	0.05
Phase errors	0.01	0.01
RSS Combination	0.24	0.24

SUMMARY

Planar near-field techniques can be used to obtain absolute gain, EIRP, and saturating flux density. The errors in such measurements are determined by the same parameters that affect far-field measurements, the gain of the standard, various insertion loss quantities, and power levels. When used on a system where these quantities are well-known, the uncertainties can be less than for similar far-field tests.

REFERENCES

[1] D. M. Kerns, *Plane-Wave Scattering-Matrix Theory of Antennas and Antenna-Antenna Interactions*. Nat. Bur. Stand., Monograph 162; June 1981.

[2] A. G. Repjar, A. C. Newell, and M. H. Francis, "Accurate determination of planar near-field correction parameters for linearly polarized probes," *IEEE Trans. Antennas Propagat.*, pp. 855-868, this issue.

[3] A. C. Newell, "Planar near-field measurement techniques," Nat. Bur. Stand., Tech. Note.

Allen C. Newell (M'78-M'81-SM'83), for a photograph and biography please see page 733 of this issue.

Robert D. Ward was born in Knoxville, TN. He received the B.S.E.E. and M.S.E.E. degrees from the University of Illinois, Urbana, in 1970 and 1971, respectively.

From 1971 to 1976 he was with Hughes Aircraft Company El Segundo, CA, where he was a Project Engineer in the Systems Test Department. He was involved in communications testing on the INTELSAT IV, HS 333, and GMS satellite programs. From 1976 to 1982 he was a Senior Project Engineer with the Antenna Department. He was involved with the design of antennas for communications satellites. In 1982 he joined the System Test Engineering Laboratory where he headed a project to engineer a planar near-field facility for the INTELSAT VI satellite program. He is currently head of the RF Engineering Section and is involved with testing of satellite antennas and communications systems.

Edward J. McFarlane was born in Pittsburgh, PA, in 1959. He received the B.S.E.E. degree from Bucknell University, Lewisburg, PA, and the M.S.E.E. degree from the University of Southern California in Los Angeles, in 1982 and 1984, respectively.

He joined the Hughes Aircraft Company, El Segundo, CA, in 1982, where he has worked in the RF test section of the System Test Engineering Laboratory. As a Project Engineer he is presently responsible for the RF systems test program for the INTELSAT VI communications satellite. In this capacity he is involved in communications and antenna subsystem tests as well as work in the systems test planar near-field facility.